Structure and Three-Dimensional Crystal Packing Preferences for *mer*-Tris(8-quinolinolato)Indium(III) Vapor-Phase-Grown Crystals

Linda S. Sapochak,*[,†,§] Asanga Ranasinghe,[†] Holger Kohlmann,[‡] Kim F. Ferris,[§] and Paul E. Burrows[§]

Departments of Chemistry and Physics, Unversity of Nevada, Las Vegas, Nevada 89154, and Pacific Northwest National Laboratory, Richland, Washington 99352

Received July 30, 2003. Revised Manuscript Received November 20, 2003

Evaluation of indium(III) tris(8-quinolinolato) (Inq_3) chelate crystals grown slowly from the vapor phase under vacuum ($\sim 10^{-6}$ Torr) was compared to the aluminum analogue, Alq_3. In both cases, a previously unidentified close $\pi-\pi$ interaction is identified, which likely impacts charge conduction. In the case of Inq_3, we observe a mixture of both meridianal (*mer*) and facial (*fac*) crystals. The larger pseudohexagon *mer*-Inq_3 crystals were analyzed by single-crystal X-ray diffraction and showed average In−N and In−O bond lengths significantly longer (0.22 and 0.26 Å, respectively) than Alq_3 and bond angles about the In^{3+} ion more distorted from an ideal octahedral geometry. The crystalline packing of *mer*-Inq_3 is found to closely resemble the β-Alq_3 phase, where both metal chelates are characterized by pairing of symmetry-related *mer*-optical isomers in three-dimensional $\pi-\pi$ stacking interactions ($\sim$3.5 Å or less). The smaller needlelike crystals were determined to be pure *fac*-Inq_3 by powder X-ray diffraction studies. An equivalent is not observed when Alq_3 is processed in an identical manner.

Introduction

Metal tris(8-quinolinolato) (Mq_3) chelates are important materials in analytical chemistry[1] and as electroluminescent emitters and hosts in organic light-emitting devices (OLEDs).[2−4] Because of the asymmetrical nature of the 8-quinolinolato ligand, two chiral geometric isomers are possible in Mq_3 chelates, meridianal (*mer*) and facial (*fac*) with C_1 and C_3 symmetries, respectively. In the case of aluminum tris(8-quinolinolato) (Alq_3), researchers have speculated that the amorphous nature and morphological stability of thermally sublimed films of Alq_3 are likely due to the presence of both isomers.[3] Calculated total energies have shown the *fac* isomer to be higher in energy compared to the *mer* form by $\sim$4−8 kcal/mol.[5−8] Theoretical and experimental (vibrational) analysis predicted that, if present, the amount of facial isomer would be <0.01% based on thermodynamic energetics.[6] However, evidence for the existence of an unspecified percentage of *fac*-Alq_3 in the δ-phase based on powder X-ray diffraction studies have been reported.[9]

There are likely implications on the conduction process in OLEDs because of the potential presence of both *mer*- and *fac*-Alq_3 in vapor-deposited films. Previous estimations of electron trap energies based on the difference between the adiabatic and vertical electron affinities suggested that the *fac*-isomer would act as a trap, limiting charge conduction processes during OLED operation,[5] though a recent report shows that such calculations are highly dependent on the chosen method and basis set.[8]

Replacement of the small Al^{3+} ion with the larger In^{3+} ion to form Inq_3 results in a metal chelate characterized by high fluxionality in solution based on both kinetic studies of isotopically labeled ligands[10] and ^{1}H NMR studies.[11,12] Unlike Alq_3 which exhibits a complicated ^{1}H NMR spectrum, Inq_3 exhibits six sharp and well-separated proton resonances in solution at room temperature, which could be misconstrued as evidence of the more symmetrical *fac* isomer.[11,12] The possibility that Inq_3 is facial in solution was ruled out because the chemical shift value of H2 (located next to pyridyl nitrogen) did not reflect the strong ring current effects

* To whom correspondence should be addressed.
[†] Department of Chemistry, University of Nevada, Las Vegas.
[‡] Department of Physics, University of Nevada, Las Vegas.
[§] Pacific Northwest National Laboratory.

(1) Hollingshead, R G. W. *Oxine and Its Derivatives*, Vol. I−IV, Butterworths: London, 1954.
(2) Tang, C. W.; VanSlyke, S. A. *Appl. Phys. Lett.* **1987**, *51*, 913.
(3) Chen, C. H.; Shi, J. *Coord. Chem. Rev.* **1998**, *171*, 161.
(4) Sapochak, L. S.; Padmaperuma, A.; Washton, N.; Endrino, F.; Schmett, G.; Marshall, J.; Fogarty, D.; Burrows, P. E.; Forrest, S. R. *J. Am. Chem. Soc.* **2001**, *126*, 6500.
(5) Curioni, A.; Boero, M.; Andreoni, W. *Chem. Phys. Lett.* **1998**, *294*, 263.
(6) Kushto, G. P.; Iizumi, Y.; Kido, J.; Kafafi, Z. H. *J. Phys. Chem.* **2000**, *104*, 3670.
(7) Martin, R. L.; Kress, J. D.; Campbell, I. H.; Smith, D. L. *Phys. Rev. B* **2000**, *61*, 15804.
(8) Ferris, K. F.; Sapochak, L. S.; Rodovsky, D.; Burrows, P. E. *Proc. Mater. Res. Soc., Org. Polym. Mater. Devices* **2003**, *771*, L3.3.
(9) Cölle, M.; Dinnebier, R. E.; Brütting, W. *Chem. Commun.* **2002**, 2908.
(10) Saito, K.; Takahashi, M.; Miyakawa, Y.; Masuda, K. *Bull. Chem. Soc. Jpn.* **1968**, *41*, 1139−1142.
(11) Green, M. A.; Huffman, J. C. The Molecular Structure of Indium Oxine. *J. Nucl. Med.* **1988**, *27*, 417−420.
(12) Addy, P.; Evans, D. F.; Sheppard, R. N. *Inorg. Chim. Acta* **1987**, *127*, L19.

10.1021/cm034709r CCC: $27.50
Published on Web 01/06/2004

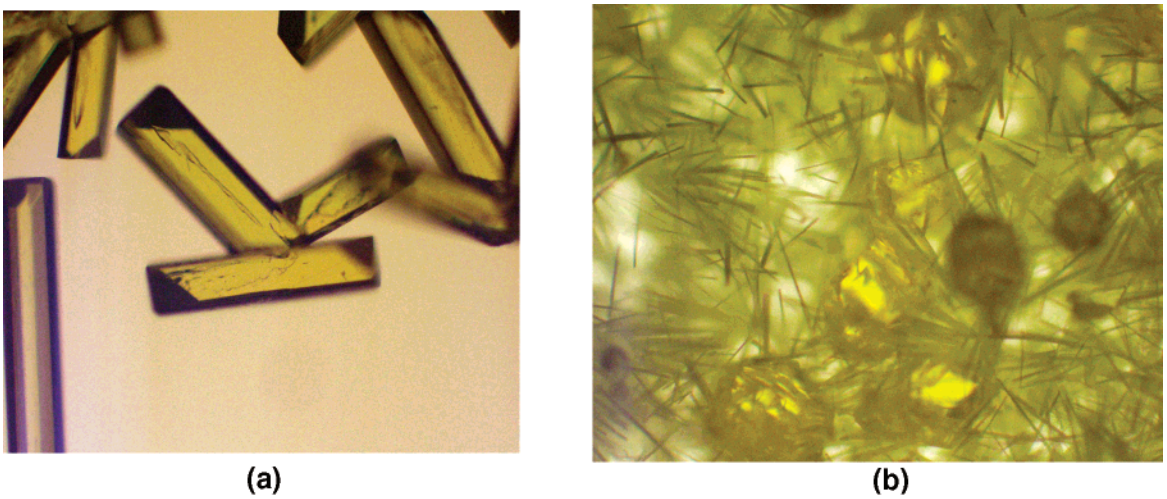

Figure 1. Optical images obtained on an Olympus BX41 optical microscope, for Inq_3 crystals: (a) crystallized from methanol and (b) grown from the vapor phase.

expected for a facial geometry, where all three H2's lie above adjacent ligand planes.[13] The explanation provided for the simplified NMR spectrum of Inq_3 was that it was completely fluxional in solution, even at room temperature.

Single-crystal X-ray diffraction studies of Inq_3 crystallized from ethanol to give Inq_3EtOH showed the geometry of Inq_3 to be meridianal.[11,14] However, it might be expected that the high fluxionality about the larger In^{3+} ion could facilitate a *mer*/*fac* conversion under thermal sublimation conditions if such conversion occurs in any of the Mq_3 chelates. Recent ab initio calculations of Inq_3 indicated the energy difference between *mer* and *fac* was indeed smaller (3.90 kcal/mol) compared to Alq_3, suggesting that for Mq_3 chelates, Inq_3 would be more likely to form the *fac*-isomer.[8] In agreement with these predictions, Rajeswaran et al. recently reported the single-crystal structure for *fac*-Inq_3 grown from the vapor phase, but crystals were poor, resulting in a relatively high R_{int} value (0.112).[15] No details of the ^1H NMR characterization were provided.

In this paper, we report the growth of both *mer*- and *fac*-Inq_3 crystals from the vapor phase. The larger crystals of *mer*-Inq_3 were characterized by single-crystal X-ray diffraction and are shown to exhibit crystalline packing practically identical to the β-phase of Alq_3, reported by Brinkmann.[16] In addition, we show that both β-Alq_3 and β-Inq_3 exhibit three-dimensional $\pi-\pi$ interactions between symmetry-related ligands. This is the first report of the crystal structure determination of unsolvated *mer*-Inq_3. Powder X-ray diffraction of the smaller crystals showed them to be facial by comparison with a recently reported crystal structure of *fac*-Inq_3.[15] Both the *mer*- and *fac*-Inq_3 crystals exhibited similar solution ^1H and ^{13}C NMR spectra consistent with the metal chelate being completely fluxional on the NMR time scale.

(13) Baker, B.; Sawyer, D. *Anal. Chem.* **1968**, *40*, 1945.
(14) Kober, N.; Achour, B.; Nepveu, F. *J. Chem. Crystallogr.* **1994**, *24* (10), 685.
(15) Rajeswaran, M.; Jarikov, V. V. *Acta Crystallogr. E* **2003**, *E59*, m306.
(16) Brinkmann, M.; Gadret, G.; Muccini, M.; Taliani, C.; Masciocchi, N.; Sironi, A. *J. Am. Chem. Soc.* **2000**, *122*, 5147.

Experimental Section

Material Synthesis and Characterization. All chemicals were obtained from Aldrich Chemical Co. and used without further purification unless specified otherwise. Indium tris-(8-quinolinolato) was prepared by first dissolving 10.00 g (130.0 mmol) of ammonium acetate and 2.80 g (7.2 mmol) of indium nitrate hexahydrate in 100 mL of deionized water. A solution of 3.20 g (22.0 mmol) of 8-quinolinol (recrystallized from 95% ethanol) dissolved in 200 mL of 1 M acetic acid was added dropwise and stirred for 40 min. The yellow precipitate was filtered, washed with water, air-dried, and then recrystallized from methanol to yield 3.66 g (86%) of a yellow crystalline solid (Inq_3MeOH), which was purified by high-vacuum gradient temperature sublimation to give *mer*- and *fac*-Inq_3. ^1H NMR (400 MHz, $CDCl_3$, 25 °C) δ H2 (J2,3) = 8.55 (d) (3.98); δ H3 (J3,4, J3,2) = 7.40 (dd) (8.14, 4.70); δ H4 (J4,3) = 8.28 (d) (8.19); δ H5 (J5,6) = 7.18 (d) (7.82); δ H6 (J6,7) = 7.50 (t) (8.00); δ H7 (J7,6) = 7.04 (d) (8.08). ^{13}C NMR (400 MHz, $CDCl_3$, 25 °C): δ C2 (145.1); δ C3 (121.1); δ C4 (140.1); δ C5 (111.9); δ C6 (130.8); δ C7 (114.8); δ C8 (159.4); δ C9 (138.4); δ C10 (130.2). Elemental analysis (NuMega Resonance Laboratories) for $C_{27}H_{18}InN_3O_3$ (547.28): calculated, C 59.26%, H 3.32%, N 7.68%; experimental, C 59.28%; H 3.30%; N 7.69%.

Single-Crystal Growth. The recrystallized material (Inq_3MeOH) was placed in a borosilicate glass tube (diameter 1 in., length 29.5 in., closed at one end), which was placed inside a larger quartz tube (diameter 2 in., closed at one end). The material was placed under vacuum ($\sim10^{-6}$ to 10^{-7} Torr) and heated in zone 3 of a Lindberg Blue 3-zone furnace at 100 °C overnight to remove solvent (zones 1 and 2 were set to 30 °C throughout the process). The temperature of zone 3 was increased slowly to a maximum temperature of 290 °C over an 8-day period. At 226 °C (day 3) a yellow film was observed in zone 1, at 242 °C (day 5) small needles were observed in zone 2, and finally at 290 °C (day 8) larger crystals were observed mixed with smaller crystals in zone 2. Crystals were removed and analyzed from zone 2 only. Crystal growth over shorter periods of time (1−3 days) yields predominately needlelike crystals.

Optical images of Inq_3 crystals grown from methanol solution to give $Inq_3(MeOH)$ and from the vapor phase to give pure *mer*- and *fac*-Inq_3 are shown in Figure 1. The crystals formed from methanol were well-defined yellow plates, consistent with previous reports for $Inq_3(EtOH)$,[11,14] whereas crystals grown from the vapor phase were composed of two types of crystals, small yellow needles and larger yellow, pseudohexagonally shaped crystals.

X-ray Single-Crystal Structure Determination of β-Inq_3. Several of the pseudohexagonally shaped crystals of Inq_3 were investigated by X-ray single-crystal diffraction. The best

Table 1. Comparison of Experimental and Theoretical Structural Parameters for β-Phases of *mer*-Inq_3 and *mer*-Alq_3

empirical formula	$C_{27}H_{18}AlN_3O_3$[16]	$C_{27}H_{18}AlN_3O_3$ (LDA)	$C_{27}H_{18}InN_3O_3$(exptl)	$C_{27}H_{18}InN_3O_3$ (LDA)
fw	409.43	409.43	547.26	547.26
crystal system	triclinic	triclinic	triclinic	triclinic
space group	$P\bar{1}$	$P\bar{1}$	$P\bar{1}$	$P\bar{1}$
a, Å	8.4433(6)	8.328	8.4815(6)	8.359
b, Å	10.2522(8)	10.186	10.3948(7)	10.324
c, Å	13.1711(10)	13.062	13.2348(9)	13.176
α, deg	108.578(1)	108.23	108.763(6)	108.46
β, deg	97.064(1)	96.53	97.664(6)	96.90
γ, deg	89.743(1)	91.68	90.375(6)	91.44
V, Å^3	1071.7(2)	1043.16	1093.43(13)	1068.2
Z	2	2	2	2
F(000)	476		548	
D(calcd), g/cm^3	1.424		1.662	
μ, mm^{-1}	0.13		1.117	
temp, K	293(2)		293(2)	
λ, Å	0.71073		0.71070	
2θ range, deg	4−58		6.06−71.70	
agreement indices	R1 = 0.059		R1 = 0.0520	

results yielded a nearly isometric crystal of dimensions 250 × 200 × 200 μm^3. Single-crystal X-ray diffraction data were collected at 297 K on a Rigaku single-crystal X-ray diffractometer equipped with an 18-kW rotating anode X-ray generator, graphite monochromator (Mo Kα radiation, λ = 0.71070 Å), 2-circle goniometer, and an image plate (30 cm × 30 cm) detector Rigaku R-axis 4++. Six hundred fifty-six frames of diffraction data were collected within the limits of 6° < ω < 334° by an ω-scan technique (step size $\Delta\omega$ = 0.5°) with the sample−detector distance fixed at 7 cm and with a beam exposure of 2 min/frame. Data were processed by the software Crystal Clear for integration with an internal residual of R_σ = 0.0196, yielding in 7871 unique reflections for the unit cell (see Table 1). Reflection data were corrected empirically for absorption effects (μ = 1.117 mm^{-1}). The structure was solved in space group type $P\bar{1}$ and refined using the program SHELX97.[17] Indium and some of the oxygen, nitrogen, and carbon atoms were found with the Patterson method. Difference Fourier maps in subsequent refinements revealed the positions of all remaining oxygen, nitrogen, and carbon atoms. Using all 7871 unique reflections in a full-matrix least-squares crystal structure refinement against F_o^2 with isotropic thermal displacement parameters yielded in agreement factors R1 = 0.0897, wR2 = 0.2502, and *S* = 1.940 for 138 refined parameters. The residuals dropped to R1 = 0.0574, wR2 = 0.1486, and *S* = 1.144 when introducing anisotropic thermal displacement parameters for all atoms, resulting in 308 refined parameters. In the last cycles of the refinement hydrogen atoms were introduced, riding on carbon atoms at fixed distances of 0.93 Å with fixed H−C−C angles of 120° and isotropic thermal displacement parameters equal to the equivalent thermal displacement parameters of the carbon atoms they were riding on. Residuals dropped again to R1 = 0.0520, wR2 = 0.1258, and *S* = 1.049.

Powder X-ray Diffraction (XRD) Studies. XRD patterns were obtained on a Philips X'pert MPD X-ray diffractometer using Cu Kα (1.54059 Å) radiation with the X-ray generator operating at 40 kV and 50 mA. The samples were prepared by packing ~10 mg of solid in a 9.0-mm cavity mount. Digital data were obtained for a 2θ range 3−36° at an angular resolution of 0.008°/s with a total counting time of 68 min.

Computational Methods. First-principles DFT computations were performed using the CASTEP electronic structure program in the Cerius2 program system.[18] Equilibrium unit cell and structural parameters were obtained from force optimization methods using the local density approximation (LDA). The exchange-correlation energies were performed using the Perdew−Zunger parametrization of the numerical results of Ceperley and Alder.[19] Initial starting structures were taken from experimental determinations. Electronic structure computations utilized a plane wave basis set with an initial 300-eV cutoff energy and ultrasoft pseudopotentials followed by subsequent refinement at a 340-eV cutoff energy. At this latter cutoff energy the finite basis set correction was less than 0.1 eV/atom.

Results and Discussion

Single-Crystal Structure Analysis of β-Inq_3. The crystal structure results for the large vapor-grown crystals of Inq_3 and structural parameters calculated from first principles are reported in Table 1 and are compared to previous results reported for solvent-free Alq_3 (β-phase) crystals grown from acetone.[16] To facilitate a comparison between Inq_3 and Alq_3 crystal structures, the ligands are labeled A, B, and C, consistent with the convention established by Brinkman et al.[16] for Alq_3 and the carbon atoms are numbered based on IUPAC numbering rules for heterocyclic rings (see Figure 2).

Identical to Alq_3, the 8-quinolinolato ligands in Inq_3 are arranged in a *meridianal* configuration about the In^{3+} ion, giving triclinic crystals belonging to space group $P\bar{1}$. Two neutral molecules compose the unit cell in both metal chelates, but unit cell parameters, volume, and density are increased for Inq_3 because of the larger In^{3+} ionic radius (0.80 Å)[20] compared to Al^{3+} (0.54 Å).[20] This is also reflected in the average In−O (2.12 Å) and In−N (2.26 Å) bond lengths, which are significantly longer (0.26 and 0.21 Å, respectively) compared to average Al−O (1.85 Å) and Al−N (2.05 Å) bond lengths in Alq_3.[16] In addition, the difference between M−N and M−O bond lengths is smaller on average (~0.14 Å) for Inq_3 compared to Alq_3 (~0.20 Å). This results in a stronger (but not closer) overlap of adjacent ligands in the crystalline packing structure of Inq_3, as discussed later.

First-principles electronic structure calculations were performed on the solvent free Inq_3 structure using the experimental determination as the starting point for the structural parameter optimization. The resulting cell parameters listed in Table 1 showed good agreement

(17) Sheldrick, G. M. *SHELX-97: A program for crystal structure determination*; University of Gottingen: Germany, 1997.

(18) (a) *CASTEP*, Materials Studio CASTEP version 2.0; Accelrys Inc.: San Diego, CA, 2001. (b) Milman, V.; Winkler, B.; White, J. A.; Pickard, C. J.; Payne, M. C.; Akhmatskaya, E. V.; Nobes, R. H. *Int. J. Quantum Chem.* **2000**, *77*, 895.

(19) (a) Perdew, J. P.; Zunger, A. *Phys. Rev. B* **1981**, *23*, 5048. (b) Ceperley, D. M.; Alder, B. J. *Phys. Rev. Lett.* **1980**, *45*, 566.

(20) *CRC Handbook of Chemistry and Physics*; Lide, D. R., Ed.; CRC Press: Boca Raton, FL, 1995; pp 12/14−12/15.

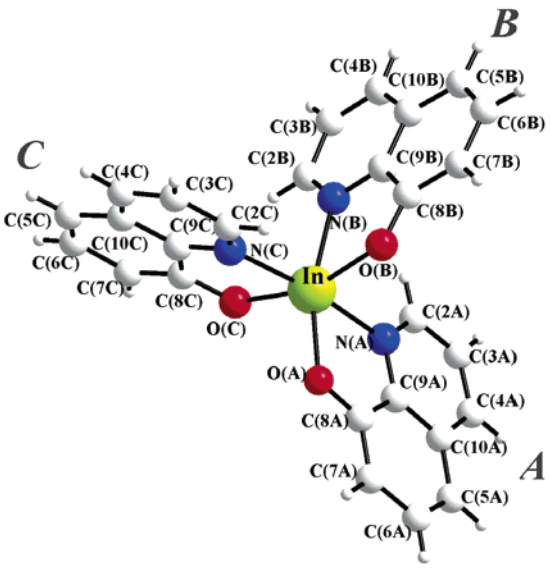

Figure 2. Structure of *mer*-Inq$_3$ with ligands labeled *A*, *B*, and *C* according to conventions reported elsewhere, heteroatoms labeled according to ligand type, and carbon atoms numbered according to IUPAC convention and differentiated by ligand type.

with experimental values, especially considering that LDA computations typically underestimate bond lengths and cell volumes. These deviations are consistent with a comparable LDA computation performed on the Alq$_3$ compound, which used the solvent-free Brinkmann structure as its starting point.[16] Comparisons of calculated bond lengths and angles for Inq$_3$ (Table 2) showed similar good agreement (<2% deviation) with the experimental determination. The In−N bond lengths are in excellent agreement, whereas Hartree−Fock molecular calculations tend to overestimate this quantity. These differences may be due to solid-state packing effects. Notably, the spatial relationships between the two molecules in the unit cell are preserved, illustrating the $\pi-\pi$ stacking interaction discussed later in this paper.

Brinkmann et al.[16] previously reported that there was little difference between bond lengths (<0.2 Å change) and bond angles (<2° change) when comparing the molecular structures of β-Alq$_3$ with the alcohol occluded crystal, Alq$_3$MeOH.[21] This is also true when comparing average In−O and In−N bond lengths of Inq$_3$ with Inq$_3$EtOH.[11,14] For both solvent-free Mq$_3$ chelates, a shortening of the M−O(*C*) bond length by ∼0.025 Å is observed because of the absence of H-bonding with the occluded solvent, which occurs with the phenolato oxygen on ligand *C* in both Alq$_3$MeOH and Inq$_3$EtOH. The bond angles of β-Alq$_3$ and Alq$_3$MeOH do not vary by much more than 2°. However, larger deviations were observed when comparing Inq$_3$ and Inq$_3$EtOH, most likely, because of the larger size of the occluded alcohol. The largest change was observed for the cis angle O(A)−In−N(C), which decreased by ∼11° in the Inq$_3$ crystal.

The geometry of both Mq$_3$ chelates is quite distorted from a typical octahedral geometry, resulting in O(C)−M−O(B), N(B)−M−O(A), and N(C)−M−N(A) trans bond angles farther from the ideal angle of 180° for

Table 2. Experimental and Theoretical Structural Parameters for *mer*-Inq$_3$

bond	length (Å) exptl.	length (Å) LDA
In−O(A)	2.1137(18))	2.146
In−O(C)	2.1138(18)	2.156
In−O(B)	2.1243(18)	2.167
In−N(C)	2.244(2)	2.229
In−N(A)	2.269(2)	2.255
In−N(B)	2.282(2)	2.261
angle	**degrees exptl.**	**degrees LDA**
O(A)−In−O(C)	101.29(9)	101.84
O(A)−In−O(B)	97.57(8)	97.37
O(C)−In−O(B)	160.51(8)	160.54
O(A)−In−N(C)	101.07(7)	101.50
O(C)−In−N(C)	77.10(7)	76.95
O(B)−In−N(C)	94.59(7)	96.33
O(A)−In−N(A)	76.70(8)	76.27
O(C)−In−N(A)	95.25(7)	93.90
O(B)−In−N(A)	93.78(7)	92.58
N(C)−In−N(A)	171.56(7)	171.03
N(B)−In−O(A)	163.41(8)	163.59
O(C)−In−N(B)	87.29(8)	86.65
O(B)−In−N(B)	75.72(7)	75.51

Inq$_3$ [161.09(9)°, 163.61(10)°, and 171.67(8)°, respectively] compared with Alq$_3$ [168.22(8)°, 171.46(8)°, and 173.82(8)°, respectively]. The cis bond angles range from 75.87(10)° to 100.98(10)° for Inq$_3$, which are farther from the ideal angle 90° compared to Alq$_3$ [range from 81.37(8)° to 97.52(7)°.][16]

Crystalline Packing in *mer*-β-Mq$_3$ Chelates. Previously, Alq$_3$ was shown to exhibit different types of crystalline packing preferences, leading to the identification of four polymorphic (α, β, γ, δ) phases.[16,22] The crystalline packing of Inq$_3$ reported here is comparable to the β-phase of Alq$_3$, as shown in Figure 3a. For both metal chelates, all three ligands are involved in close $\pi-\pi$ interactions (3.5 Å or less) of symmetry-related 8-quinolinolato ligands, but how the rings overlap and which atoms show close interactions is different for each ligand and for both metal chelates, as shown in Figure 3b−d.

The closest $\pi-\pi$ stacking interactions in both β-Alq$_3$ and β-Inq$_3$ occur between ligands *C*/*C*′ (represented in yellow, Figure 3), where the pyridyl ring of ligand *C* lies above the center of the symmetry-related *C*′ ligand, resulting in both pyridyl ring/pyridyl ring and pyridyl ring/phenolato ring overlap, as depicted previously for β-Alq$_3$.[16] Stronger overlap between the *C*/*C*′ ligands was observed for β-Inq$_3$ where close interactions occur between several atoms [C3/C8′ (3.38 Å), N/C10′ (3.43 Å), C2/C5′ (3.45 Å), and C9/C4′ (3.46 Å)]. The shortest atomic distances were observed between C2/C5′ and C9/C4′ (both 3.38 Å) for β-Alq$_3$, but all other atomic interactions were >3.5 Å.

The stacking interactions of ligands *B*/*B*′ (represented in pink, Figure 3) for both β-Alq$_3$ and β-Inq$_3$ were characterized by a stronger pyridyl ring/phenolato ring overlap, similar to that described previously for tetrameric Znq$_2$.[23] The closest interactions of ligands *B*/*B*′

(21) Schmidbaur, H.; Lattenbauer, J.; Dallas, L.; Muller, W. G.; Kumberger, O. *Z. Naturforsh.* **1991**, *46b*, 901.

(22) Braun, M.; Gmeiner, J.; Tzolov, M.; Coelle, M.; Meyer, F. D.; Milius, W.; Hellebrecht, H.; Wendland, O.; von Schutz, J. U.; Brutting, W. *J. Chem. Phys.* **2001**, *114*, 9625−9632.

(23) Sapochak, L. S.; Benincasa, F. E.; Schofield, R. S.; Baker, J. L.; Riccio, K. K.; Fogarty, D.; Kohlmann, H.; Ferris, K. F.; Burrows, P. E. *J. Am. Chem. Soc.* **2002**, *124*, 6119.

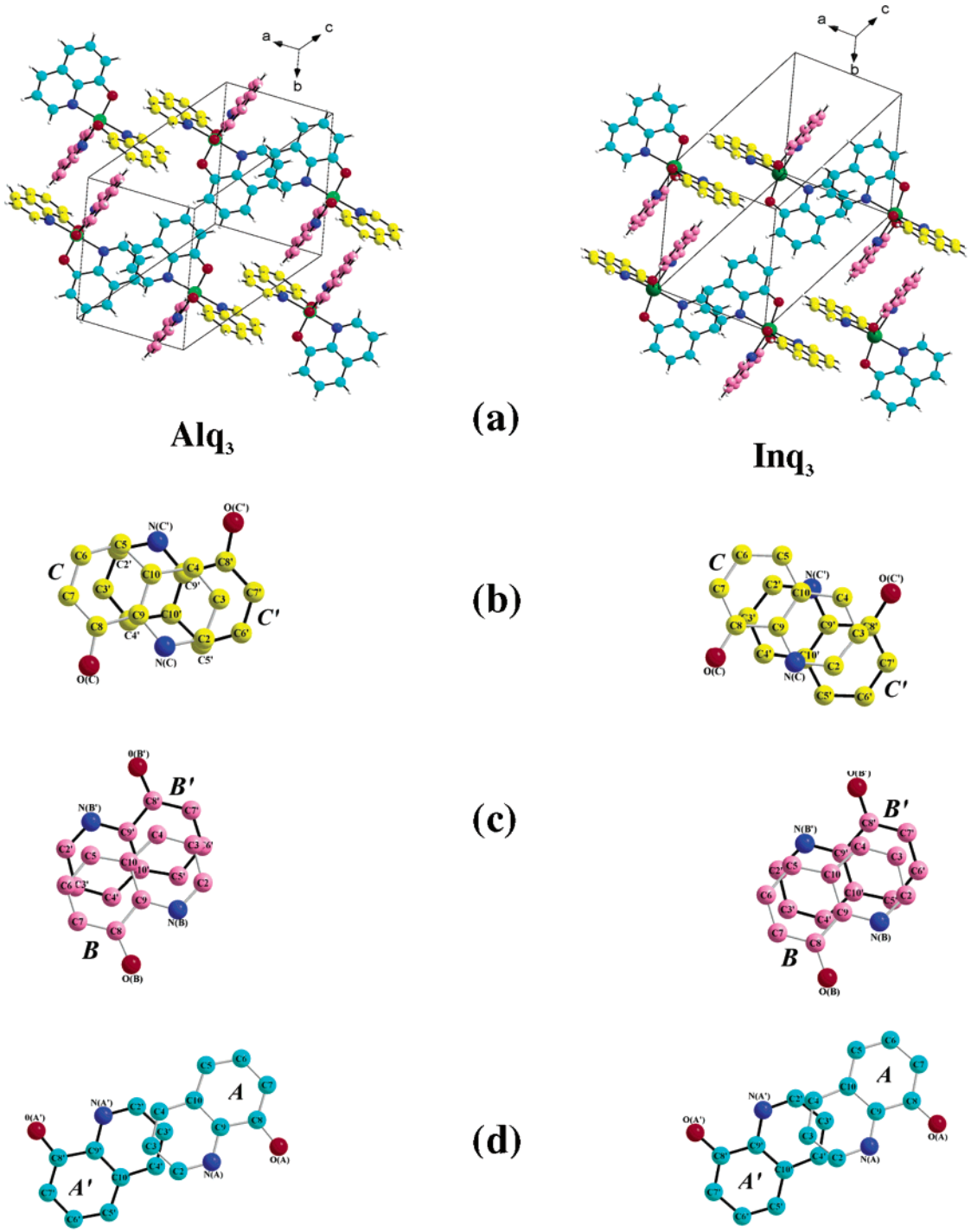

Figure 3. 3-D crystalline packing is shown in (a) for β-Alq$_3$ and β-Inq$_3$ with ligands *A* in blue, ligands *B* in pink, and ligands *C* in yellow. The nature of the $\pi-\pi$ stacking interactions between enantiomeric pairs is shown in (b) for ligand *C* and *C*′, (c) for ligand *B* and *B*′, and (d) for ligands *A* and *A*′.

for β-Alq$_3$ were observed between C10/C10′ and C3/C6′ (both ~3.45 Å). This is in contrast to the previous description of β-Alq$_3$ $\pi-\pi$ stacking interactions, which indicated that the strongest interactions were between pyridyl rings.[16] On the other hand, in β-Inq$_3$ the stacking interactions of ligands *B*/*B*′ were more similar to those of *C*/*C*′ described for β-Alq$_3$, with the closest interactions between atoms C2/C5′ and C9/C4′ (both ~3.50 Å).

On further inspection of the crystallographic packing of both β-Alq$_3$ and β-Inq$_3$, we identified a third close $\pi-\pi$ interaction (~3.50 Å) between symmetry-related ligands *A*/*A*′ (represented in blue, Figure 3). The overlap is much weaker than the other interactions and occurs between atoms C3, C2, and C4 of the pyridyl rings only where the closest interactions were between atoms C3/C3′ (3.50 Å) in β-Alq$_3$ and between C2/C4′ (3.56 Å) in β-Inq$_3$ (see Figure 3d).

Powder X-ray Diffraction Results for *fac*-Inq$_3$. The small needle crystals (as shown in Figure 1b) grown slowly in this report were too small to obtain single-crystal diffraction data, but a comparison of the powder X-ray diffraction pattern and the diffraction patterns for *mer*- and *fac*-Inq$_3$ generated from the single-crystal

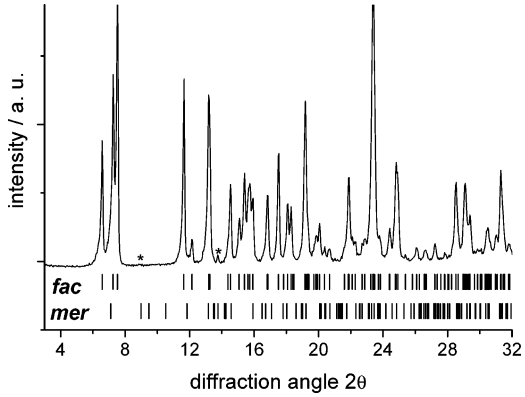

Figure 4. A comparison of the experimental powder XRD pattern for small needlelike crystals of Inq_3 grown from the vapor phase with the theoretically calculated patterns for *fac*-Inq_3[12] and *mer*-Inq_3. Experimental reflections that do not appear in the theoretical pattern for the *fac*-isomer are starred.

structural data are shown in Figure 4. It is clear that the small needles exhibit a diffraction pattern most consistent with the facial isomer. However, some small reflections were observed in the experimental pattern which did not appear in the theoretically generated pattern for *fac*-Inq_3 (see starred reflections in Figure 4), suggesting that the *mer*-isomer may coexist as a minor component with the facial form. Longer growth time resulted only in the formation of larger crystals of *mer*-Inq_3. Thermal interconversion between these two geometrical isomers during the crystal growth process is believed to be the reason for the inability to grow larger crystals of the *fac*-isomer. The mechanism and evidence for thermal conversion between *mer*/*fac* isomers will be reported elsewhere.

Conclusions

Crystals of both pure *mer*- and *fac*-Inq_3 were grown from high vacuum gradient temperature sublimation of *mer*-Inq_3MeOH. The crystalline packing preferences for *mer*-Inq_3 were similar to the β-phase of Alq_3; however, a third short $\pi-\pi$ stacking interaction ($\sim$3.5 Å) not identified previously for β-Alq_3 was observed for both metal chelates. A detailed description of the $\pi-\pi$ stacking interactions revealed both pyridyl ring/pyridyl ring and pyridyl ring/phenolato ring overlap, but because of the significantly longer M−N and M−O bonds lengths in β-Inq_3, the number of atoms associated with these interactions was greater for Inq_3, suggesting a more efficient overlap of adjacent ligands.

Both geometric isomers are observed upon thermal sublimation, suggesting that vapor-deposited films of Inq_3 are likely a mixture of both *mer*- and *fac*-isomers. As a result of this structural diversity, Inq_3 is a good model compound to investigate the effect of how the presence of both isomers affects charge conduction during OLED operation and will likely shed new light on conduction mechanisms in the better known analogue, Alq_3.

Acknowledgment. The authors gratefully acknowledge financial support from NSF (CAREER-DMR-9874765), DOE Cooperative Agreement (DE-FC08-01NV14049), Office of Naval Research (N00014-03-1-0247), Office of Basic Energy Sciences, U.S. Department of Energy (USDOE), and the PNNL Laboratory Directed Research and Development Program. We also thank Dr. Yong Soon Shin for conducting the XRD experiments. *Pacific Northwest National Laboratory (PNNL) is operated by Battelle Memorial Institute for the U.S. Department of Energy (DOE) under Contract DE-AC06-76RLO 1830.*

Supporting Information Available: Crystallographic information (CIF) and theoretical structural parameters. This material is available free of charge via the Internet at http://pubs.acs.org.

CM034709R